Title
Single-nanowire photoelectrochemistry

Journal
Nature Nanotechnology, 11(7)

ISSN
1748-3387

Authors
Su, Yude
Liu, Chong
Brittman, Sarah
et al.

Publication Date
2016-07-01

DOI
10.1038/nnano.2016.30

Peer reviewed

Single-Nanowire Photoelectrochemistry

Authors:

Yude Su[1†], Chong Liu[1,3†], Sarah Brittman[1,3], Jinyao Tang[1,3], Anthony Fu[1,3], Nikolay Kornienko[1,3], Qiao Kong[1], Peidong Yang[1,2,3,4*]

Affiliations:

[1] Department of Chemistry, University of California, Berkeley, CA 94720, USA

[2] Department of Materials Science and Engineering, University of California, Berkeley, CA 94720, USA

[3] Materials Sciences Division, Lawrence Berkeley National Laboratory, Berkeley, CA 94720, USA

[4] Kavli Energy Nanosciences Institute, Berkeley, CA 94720, USA

[†] These authors contributed equally to this work.

[*] To whom correspondence should be addressed. Email: p_yang@berkeley.edu

Photoelectrochemistry[1-3] is one of several promising approaches[4-5] to realize efficient solar-to-fuel conversion. Recent work has shown that photoelectrodes made of semiconductor nano/microwire arrays can have better photoelectrochemical (PEC) performance[6-8] than their planar counterparts because of their unique properties, such as high surface area[9-11]. Although much effort has been focused on studying wire arrays, inhomogeneity in the geometry, doping, defects and catalyst loading present in such arrays can obscure the link between these properties and the wires' PEC performance; correlating the performance with the specific properties of individual wire is difficult because of ensemble averaging. Here, we show that a single-nanowire-based photoelectrode platform can be used to reliably probe the current-voltage (*I-V)* characteristics of individual nanowires. We found that the photovoltage output of ensemble array samples can be limited by poorly performing individual wires, which highlights the importance of improving the nanowire homogeneity within an array. Furthermore, this platform allows the flux of photo-generated electrons to be quantified as a function of the lengths and diameters of individual nanowires, and the flux over the entire nanowire surface (7-30 electrons/ (nm^2·s)) is found to be significantly reduced as compared to that of a planar analogue (~1,200 electrons/ (nm^2·s)). Such characterization of the photo-generated carrier flux at the semiconductor/electrolyte interface is essential for designing nanowire photoelectrodes that match the activity of their loaded electrocatalysts.

Devices composed of single nanowires have previously been used in electronics[12], bio-probing[13], photovoltaics[14, 15], thermoelectrics[16] and electrochemistry[17]. In this work we developed a wellcontrolled device of single-semiconductor-nanowire (Fig. 1a) for photoelectrochemistry, which is capable of detecting solar-powered proton reduction with pico-ampere (pA) sensitivity. As a model system, silicon (Si)[18-21] and platinum (Pt)[22] are selected as the light-absorbing semiconductor and the proton-reduction electrocatalyst respectively. Si nanowires were grown epitaxially on the pre-patterned, degenerately-doped Si <111> device layer of a silicon-on-insulator (SOI) substrate, as shown in the scanning electron microscope (SEM) image (Fig. 1b). With an oxide layer underneath, the patterned Si electrodes are electrically isolated from each other, enabling the characterization of each nanowire individually. Moreover, the VLS growth allowed control over the nanowire's dimensions[23], which facilitated studying the effects of the nanowire's geometry. In this work, the as-grown single Si nanowires were 8-20 μm long and 500-800 nm in diameter. The post-growth fabrication process yielded nanowires with two types of doping profiles (Fig. 2a). In one case, the as-grown Si nanowires were doped into *p*-type only. In the second case, after the *p*-type doping, an n^+ shell was added to yield an n^+p buried junction in each single nanowire. For both types of devices, Pt nanoparticles were deposited electrolessly[22] onto the exposed nanowire (Supplementary Fig. 2, 3) after a protective polymer coating was added to the base of the wire. Additionally, a specialized PEC measurement setup was developed (Fig. 2b) for high-sensitivity electrochemical characterization coupled with simulated sunlight. This unique measurement platform can be further applied to other light-driven redox reactions that require high sensitivity.

These aforementioned techniques provide us with a nanowire photoelectrode platform that is individually addressable and enable the first observation of single-nanowire photoelectrochemistry. The photocurrents of devices were characterized with pA sensitivity (Fig.

3a). In the dark, devices show negligible current (|I| < 1 pA). The slightly increased current at potentials negative of 0 V *vs.* the reversible hydrogen electrode (RHE) implies a proton-reduction reaction catalyzed by the loaded Pt nanoparticles (Supplementary Fig. 5). Under one-sun illumination (100 mW/cm^2, AM 1.5G), a significant photoresponse was observed with the photocurrent reaching a plateau under negative bias, indicative of a light-activated process limited by the number of incident photons. Such PEC behavior is consistent with that of the reported ensemble systems[18, 19], confirming the observation of PEC phenomena at the single-nanowire level. Additionally, the performance of the device was consistent for multiple scan cycles (Fig. 3b).

The photovoltage distribution statistics of the single-nanowire devices was analyzed next. For Si photocathodes, a previous study on ensemble systems proposed that the n^+p buried junction increases the degree of band bending at the interface and consequently leads to a 250-350 mV improvement in photovoltage[18]. This concept was also implemented in our single-nanowire photoelectrodes (Supplementary Scheme 1). The onset potentials and standard deviations of *p*-Si and n^+p-Si devices are 280±110 mV and 530±120 mV *vs.* RHE, respectively (Fig. 3c). The ~250 mV difference between the average onset potentials demonstrates that the single-nanowire photoelectrode's doping profile and photovoltage can be reproducibly modulated. In addition, for devices that underwent the same growth and doping process, the broad photovoltage distribution implies individual variance among single nanowires. To investigate the impact of such variance, we carried out PEC measurements on ensemble nanowire arrays (Supplementary Fig. 6), in which many individual nanowires are connected in parallel. It was found that the V_{oc} of the array device is comparable with that of the single nanowire with the lowest photovoltage output

(Supplementary Fig. 7), and this observation applied to both *p*-Si and n^+p-Si devices (Supplementary Fig. 8, Table 1). These results suggest that the photovoltage of the ensemble array photoelectrode is largely affected by the worst-performing individual nanowire, and this conclusion is further supported by our calculation based on an equivalent circuit model (Supplementary Fig. 9). Since the single nanowires and the nanowire arrays studied in this work have similar physical dimensions and go through the same doping process, such observed individual variance should be related to the heterogeneity of the material quality introduced during either the VLS growth[24, 25] or the fabrication process, or both. As a result, our report emphasizes the importance of controlling material quality not only in the averaged value but also the sample homogeneity, in order to produce efficient nanowire-based solar-to-fuel devices.

Owing to the high-sensitivity photocurrent measurement and the well-defined geometry of a single nanowire, the photo-generated electron flux through the nanowire's entire surface ($Flux_{wire}$) was quantified. Because of the nanowire's large surface area, $Flux_{wire}$ was much reduced compared to a planar analogue. In order to quantitatively evaluate how the large surface area functions to dilute the electron flux, the roughness factor of a single nanowire (γ_{rough}) is introduced in equation (1). Here the nanowire is considered as a cylinder whose length and diameter are L and D, respectively.

$$\gamma_{rough} = \frac{\text{actual surface area of a single nanowire}}{\text{cross section area of a single nanowire}} = \frac{4L}{D} + 1 \qquad (1)$$

Subsequently, as shown in equation (2), $Flux_{wire}$ can be correlated with $Flux_{geo}$, which is the photo-generated electron flux normalized to the geometric cross-sectional area.

$$Flux_{wire} = \frac{Flux_{geo}}{\gamma_{rough}} \quad (2)$$

Therefore $Flux_{wire}$ can be expressed as a function of L and D, which allows for a quantitative calculation of $Flux_{wire}$ for each single-nanowire device. For a representative device (Fig. 4a), I reaches a plateau of -43 pA when cathodic bias is applied. Correspondingly, J and $Flux_{geo}$ are -22 mA/cm^2 and 1,350 electrons/ (nm^2·s), respectively (-1 mA/cm^2 = 62 electrons/ (nm^2·s)). When normalizing to the nanowire's actual surface area, the corresponding $Flux_{wire}$ is dramatically reduced to 13 electrons/ (nm^2·s), because of the large γ_{rough}. Compared to the photo-generated electron flux of a planar n^+p-Si electrode (1,240 electrons/ (nm^2·s) at 0V *vs.* RHE, see Supplementary Fig. 10), $Flux_{wire}$ is diluted by about 100 times. The trend of such a reduced electron flux is elucidated when values of saturated $Flux_{wire}$ for individual nanowires were plotted against their L and D (Fig. 4b). Here we take advantage of the fact that the dimensions of each single nanowire are not only highly tunable but also can be reliably measured, in contrast to the inhomogeneity that typically occurs for ensemble devices. Ranging from 30 to 7 electrons/ (nm^2·s), $Flux_{wire}$ follows a generally decreasing trend as L becomes longer or D becomes smaller (Supplementary Fig. 11). Such dependence can be clearly seen when $Flux_{wire}$ is correlated with γ_{rough}, which incorporates the impact of both L and D (Fig. 4c). $Flux_{wire}$ tends to decrease as γ_{rough} increases. The effective reduction of electron flux on the nanowire surface can be estimated by considering the light absorption within a cylindrical silicon absorber, and is found to scale with the γ_{rough} of the individual nanowires (Supplementary Fig. 13).

The characterization of $Flux_{wire}$ provides quantitative insight into the nanowire geometry's benefits in photoelectrochemistry. In principle, the loaded electrocatalyst should have a sufficiently high TOF to handle the photo-generated electron flux[11]. As a result, the much reduced $Flux_{wire}$ (7-30 electrons/ $(nm^2 \cdot s)$ under 1 Sun illumination measured in this study, compared to typical ~1,200 electrons/ $(nm^2 \cdot s)$ for a planar photoelectrode) can significantly alleviate the requirement on the TOFs of loaded electrocatalysts and consequently reduce the necessary overpotential as compared with a planar counterpart (see Supplementary Table 2 for specific values). This is especially critical for more complicated and sluggish electrochemical reactions such as CO_2 reduction[26, 27], where the electrocatalyst typically needs a large overpotential to reach an appreciable TOF[28-30]. In addition, the systematic trend of $Flux_{wire}$ introduces the possibility to design specific nanowire geometries to match the activities of different loaded electrocatalysts in different PEC reactions. This single-nanowire photoelectrode represents a model system that can be used to study and design nanowire photoelectrodes for next-generation solar-to-fuel conversion devices.

References

1. Bard, A. J. Photoelectrochemistry. *Science* **207**, 139-144 (1980)
2. Grätzel, M. Photoelectrochemical cells. *Nature* **414**, 338-344 (2001).
3. Walter, M. G. *et al.* Solar water splitting cells. *Chem. Rev.* **110**, 6446-6473 (2010).
4. Reece, S. Y. *et al.* Wireless solar water splitting using silicon-based semiconductors and earth-abundant catalysts. *Science* **334**, 645-648 (2011).
5. Wang, H. *et al.* Semiconductor heterojunction photocatalysts: design, construction, and photocatalytic performances. *Chem. Soc. Rev*. **43**, 5234-5244 (2014).
6. Hwang, Y. J., Boukai, A. & Yang, P. High density *n*-Si/*n*-TiO_2 core/shell nanowire arrays with enhanced photoactivity. *Nano Lett.* **9**, 410-415 (2009).
7. Hwang, Y. J., Wu, C. H., Hahn, C., Jeong, H. E. & Yang, P. Si/InGaN core/shell hierarchical nanowire arrays and their photoelectrochemical properties. *Nano Lett.* **12**, 1678-1682 (2012).
8. Liu, R. *et al.* Silicon nanowires as photoelectrodes for carbon dioxide fixation. *Angew. Chem. Int. Ed.* **51**, 6709-6712 (2012).
9. Mayer, M. T., Lin, Y., Yuan, G. & Wang, D. Forming heterojunctions at the nanoscale for improved photoelectrochemical water splitting by semiconductor materials: case studies on hematite. *Acc. Chem. Res.* **46**, 1558-1566 (2013).
10. Wu, Y., Yan, H. & Yang, P. Semiconductor nanowire array: potential substrates for photocatalysis and photovoltaics. *Top. Catal.* **19**, 197-202 (2002)
11. Liu, C., Dasgupta, N. P. & Yang, P. Semiconductor nanowires for artificial photosynthesis. *Chem. Mater.* **26**, 415-422 (2014).
12. Cui, Y., Wei, Q., Park, H. & Lieber, C. M. Nanowire nanosensors for highly sensitive and selective detection of biological and chemical species. *Science* **293**, 1289-1292 (2001)
13. Yan, R. *et al.* Nanowire-based single-cell endoscopy. *Nature Nanotech.* **7**, 191-196 (2012).
14. Tian, B., Kempa, T. J. & Lieber, C. M. Single nanowire photovoltaics. *Chem. Soc. Rev.* **38**, 16-24 (2009)
15. Tang, J., Huo, Z., Brittman, S., Gao, H. & Yang, P. Solution-processed core-shell nanowires for efficient photovoltaic cells. *Nature Nanotech.* **6**, 568-572 (2011).
16. Hochbaum, A. I. *et al.* Enhanced thermoelectric performance of rough silicon nanowires. *Nature* **451**, 163-167 (2008).
17. Cox, J. T. & Zhang, B. Nanoelectrodes: recent advances and new directions. *Annu. Rev. Anal. Chem.* **5**, 253-272 (2012).
18. Boettcher, S. W. *et al.* Photoelectrochemical hydrogen evolution using Si microwire arrays. *J. Am. Chem. Soc.* **133**, 1216-1219 (2011).
19. Hou, Y. *et al.* Bioinspired molecular co-catalysts bonded to a silicon photocathode for solar hydrogen evolution. *Nature Mater.* **10**, 434-438 (2011).
20. Esposito, D. V., Levin, I., Moffat, T. P. & Talin, A. A. H_2 evolution at Si-based metal-insulator-semiconductor photoelectrodes enhanced by inversion channel charge collection and H spillover. *Nature Mater.* **12**, 562-568 (2013).
21. Ji, L. *et al.* A silicon-based photocathode for water reduction with an epitaxial $SrTiO_3$ protection layer and a nanostructured catalyst. *Nature Nanotech.* **10**, 84-90 (2015).
22. Gorostiza, P., Allongue, P., Díaz, R., Morante, J. R. & Sanz, F. Electrochemical characterization of the open-circuit deposition of platinum on silicon from fluoride solutions. *J. Phys. Chem. B* **107**, 6454-6461 (2003).
23. Hochbaum, A. I., Fan, R., He, R. & Yang, P. Controlled growth of Si nanowire arrays for device integration. *Nano Lett*. **5**, 457-460 (2005).
24. Allen, J. E. *et al.* High-resolution detection of Au catalyst atoms in Si nanowires. *Nature Nanotech.* **3**, 168-173 (2008).
25. Koren, E. *et al*. Direct measurement of individual deep traps in single silicon nanowires. *Nano Lett.* **11**, 2499-2502 (2011).

26. Barton, E. E., Rampulla, D. M. & Bocarsly, A. B. Selective solar-driven reduction of CO_2 to methanol using a catalyzed *p*-GaP based photoelectrochemical cell. *J. Am. Chem. Soc.* **130**, 6342-6344 (2008).
27. Kumar, B., Smieja, J. M. & Kubiak, C. P. Photoreduction of CO_2 on *p*-type silicon using Re(bipy-Bu^t)$(CO)_3$Cl: photovoltages exceeding 600 mV for the selective reduction of CO_2 to CO. *J. Phys. Chem. C.* **114**, 14220–14223 (2010).
28. Benson, E. E., Kubiak, C. P., Sathrum, A. J. & Smieja, J. M. Electrocatalytic and homogeneous approaches to conversion of CO_2 to liquid fuels. *Chem. Soc. Rev.* **38**, 89-99 (2009).
29. Appel, A. M. *et al.* Frontiers, opportunities, and challenges in biochemical and chemical catalysis of CO_2 fixation. *Chem. Rev.* **113**, 6621-6658 (2013).
30. Hori, Y. *et al.* Electrocatalytic process of CO selectivity in electrochemical reduction of CO_2 at metal electrodes in aqueous media. *Electrochim. Acta.* **39**, 1833-1839 (1994).

Acknowledgements

This work was supported by the Director, Office of Science, Office of Basic Energy Sciences, Materials Sciences and Engineering Division, of the US Department of Energy (contract no. DE-AC02-05CH11231, Pchem). High resolution transmission electron microscopy was performed at the National Center of Electron Microscopy (NCEM) in the Molecular Foundry at Lawrence Berkeley National Lab. The authors would like to acknowledge Kelsey Sakimoto, Joaquin Resasco, Andrew Wong, Dr. Samuel Eaton and Dr. Jongwoo Lim for helpful discussions. The authors thank the Marvell Nanofabrication Laboratory for use of their facilities.

Author contributions

Y. S., C. L. and P. Y. conceived and designed the experiments. Y. S., C. L., S. B. and J. T. fabricated the single-nanowire devices. Y. S. and C. L. performed the PEC measurements on single-nanowire devices. Y. S., C. L. and A. F. carried out the numerical calculation. Y. S. and Q. K. fabricated and characterized the nanowire array samples. N. K. carried out the high-resolution TEM imaging. Y. S., C. L. and P. Y. co-wrote the paper. All authors discussed the results and revised the manuscript.

Additional information

The authors declare no competing financial interests. Supplementary information accompanies this paper at www.nature.com/naturenanotechnology. Reprints and permission information is available online at http://www.nature.com/reprints. Correspondence and requests for materials should be addressed to P. Y.

Figure Captions

Figure 1. Single-nanowire photoelectrode for PEC measurements. a, Schematics of the single Si nanowire for the PEC process. Under illumination, the photo-excited electron-hole pairs are produced and subsequently separated at the nanowire/electrolyte interface because of the band bending. The electrons then move to the Pt catalytic sites and carry out the proton reduction. **b,** SEM image of the individually addressable single nanowires. The Si layer of the SOI substrate is patterned into nine electrically isolated, oxide-passivated electrodes, with an oxide layer underneath. The single Si nanowires are vertically grown on these isolated Si electrodes by the vapor-liquid-solid (VLS) mechanism[23]. The scale bar is 10 μm.

Figure 2. Schematic illustrations of the fabrication and measurement processes. a, Outline of the post-growth fabrication process (see Methods and Supplementary Fig. 1 for details). Devices with two kinds of doping profiles (p-Si and n^+p-Si) were fabricated for comparison. **b,** The PEC measurement scheme. A two-electrode configuration was used to characterize the *I*-*V* properties of single nanowires. While the Si nanowire serves as the working electrode, a Pt wire functions as the counter/reference electrode whose electrochemical potential was calibrated (Supplementary Fig. 4). The reactor volume in which the PEC processes occur is defined by a polydimethylsiloxane (PDMS) chamber. A probe makes electrical contact to each nanowire through the outside pads, while the chamber is illuminated from above.

Figure 3. PEC performance of the single-Si-nanowire devices. a, *I*-*V* characteristics of single-nanowire devices. The measurement was carried out in 0.1 M K_2SO_4 solution adjusted to pH ~ 2 with H_2SO_4. Under simulated sunlight (100 mW/cm^2, AM 1.5G), both the p-Si device ($L = 8\ \mu m, D = 620\ nm$) and n^+p-Si device ($L = 12.5\ \mu m, D = 530\ nm$) have significant photoresponses. The purple arrows indicate the onsets of photocurrent as defined in **c**. **b,** Repeated scans of the n^+p-Si device displayed in **a**. **c,** The statistical distribution of onset potentials for seven p-Si and nine n^+p-Si devices. To evaluate the photovoltage response of the single-nanowire devices, the onset potential is defined as the potential *vs*. RHE where ΔI is -0.5 pA. Here ΔI is the difference between the photocurrent and the dark current. The pink band shows the difference in the average onset potential between p-Si and n^+p-Si devices.

Figure 4. Analysis of the flux of photo-generated electrons. a, The PEC behavior of a representative n^+p-Si device ($L = 13\ \mu m, D = 490\ nm$). The four y-axes represent (from left to right) the recorded photocurrent (I), the current density based on the geometric cross-sectional area (J), the electron flux normalized to the geometric cross-sectional area ($Flux_{geo}$), and the electron flux through the nanowire's entire surface ($Flux_{wire}$), respectively. **b,** The statistical distribution of saturated $Flux_{wire}$ as a function of L and D of individual nanowires. Each data point represents a repeatable measurement of one single-nanowire device. **c,** The dependence of saturated $Flux_{wire}$ on the roughness factor of individual nanowires (γ_{rough}).

Methods

Growth of Si nanowires. The heavily doped (ρ of 0.01-0.05 Ω cm) *p*-type (boron) SOI wafers with 3 μm device layer oriented <111> and 2 μm buried oxide layer were obtained from WRS Materials. The device layer was first thinned down to 1.5 μm by thermal oxidation and subsequent etching in buffered hydrofluoric acid (BHF). Then the device layer was further doped with boron (Techneglas GS-139) at 1,050 ºC for 10 hours, followed by a second thermal oxidation and BHF etching. The resulting device layer was ~1 μm thick with a resistivity < 0.002 Ω cm. The Si electrodes were patterned by photolithography and anisotropic plasma etching (Surface Technology Systems), and then thermally oxidized to form a 300 nm thick oxide. The bonding pads were defined by photolithography and anisotropic plasma etching of the oxide (Plasma-Therm PK-12 RIE). The catalysts for VLS growth were defined by photolithography, anisotropic plasma etching of the oxide, and subsequent electron-beam evaporation of gold (150 nm). The isolated Si nanowires were grown at 875 ºC for 10-15 minutes with $SiCl_4$ as the precursor and 10% hydrogen in argon as the reducing agent.

Device fabrication after growth. The as-grown isolated Si nanowires were etched in BHF for 30 seconds and subsequently soaked in gold etchant (Transene) for 30 minutes. Then the nanowires were thermally oxidized at 1,000 ºC for 1 hour, followed by etching in BHF. The boron doping process was split into two parts. First, boron was pre-deposited at the nanowire surface at 750 ºC for 1 hour, with 1% BCl_3 in argon as the precursor and 10% hydrogen in argon as the reducing agent. Second, the boron atoms at the nanowire surface were driven into the nanowire at 1,000 ºC for 5 hours in vacuum. The resulting boron doping level of the single nanowires was estimated to be ~2×10^{17}/cm^3. Such estimation is based on the resistivity of the SOI control chip, which was approximated by four-probe measurement. The key steps used in the n^+ layer fabrication are given below (see Supplementary information for details). First, the *p*-Si nanowires were thermally oxidized at 1,000 ºC for 1 hour, then coated with ~1 μm of I-line photoresist at the base of the nanowires. Second, BHF was used to etch the oxide on the nanowire upper exposed part, followed by I-line removal in acetone. Third, a Si handle wafer was spin-coated with arsenic-containing spin-on dopant (SOD) (Filmtronics, Inc.) and baked at 150 ºC for 30 minutes. Then the device chip was placed on the SOD coated Si wafer, and annealed at 900 ºC for 4 minutes in an N_2 atmosphere to form an n^+ layer at the nanowire's surface. Fourth, SU-8 dissolved in ethyl acetate was drop-cast onto the device chip, resulting in a ~3 μm thick SU-8 layer at the base of the device chip. With the SU-8 at the bonding pad scratched to expose the electrode's surface, the chip was baked in order to harden the SU-8. Finally, after a quick etching in BHF, the device chip was soaked in the solution containing 0.1 M HF and 0.2 mM K_2PtCl_6 for 3 minutes to carry out the platinum deposition on the nanowire surface[22].

PEC measurement. A 150 W Xenon arc lamp (Newport Corporation) with an AM1.5G filter was used to characterize the PEC response of the single-nanowire devices. As a top-illumination measurement, the angle between the incident light and the axis of the single nanowire is smaller than 3º. The light intensity was calibrated using a Si photodiode referenced to an NREL calibrated Si photodiode. All PEC measurements were carried out in a two-electrode configuration. A platinum wire worked as the counter electrode, whose electrochemical potential was immediately calibrated with Ag/AgCl (0.1 M KCl) after the PEC measurement (Supplementary Fig. 4). A PDMS chamber was used to define the reactor space, where the nanowire device was immersed in 0.1 M aq. K_2SO_4 adjusted to pH ~ 2 using H_2SO_4. *I-V* characterization was performed with a Keithley 2636 source-measure unit (SMU), and the typical potential sweep rate was 10 mV/s. The open-circuit instrumental noise current level is less than 0.5 pA.

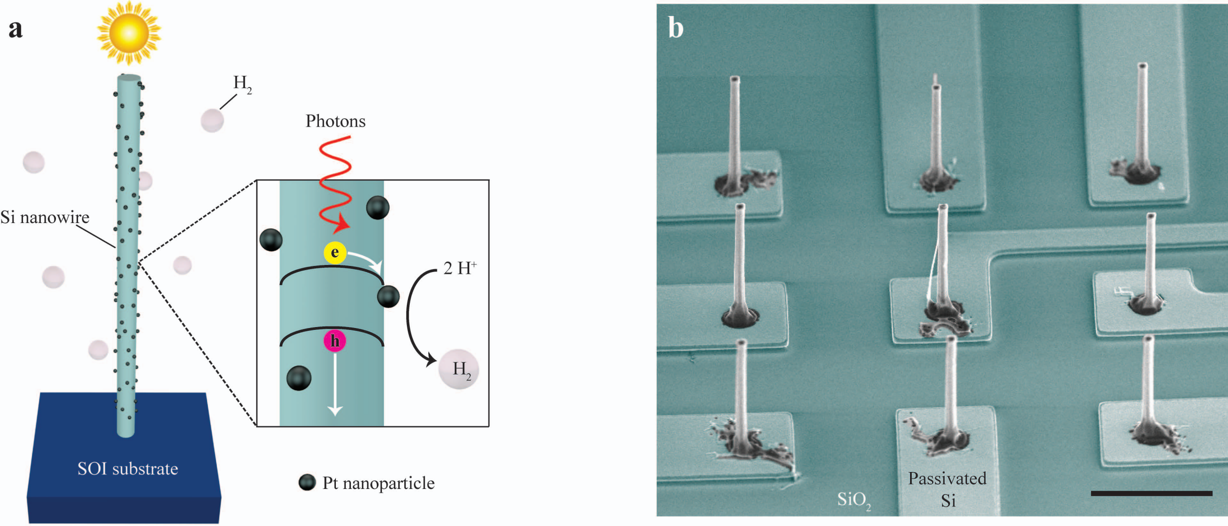
a
H2
Photons
Si nanowire
e
2 H+
h
H2
SOI substrate
Pt nanoparticle
b
SiO2
Passivated Si

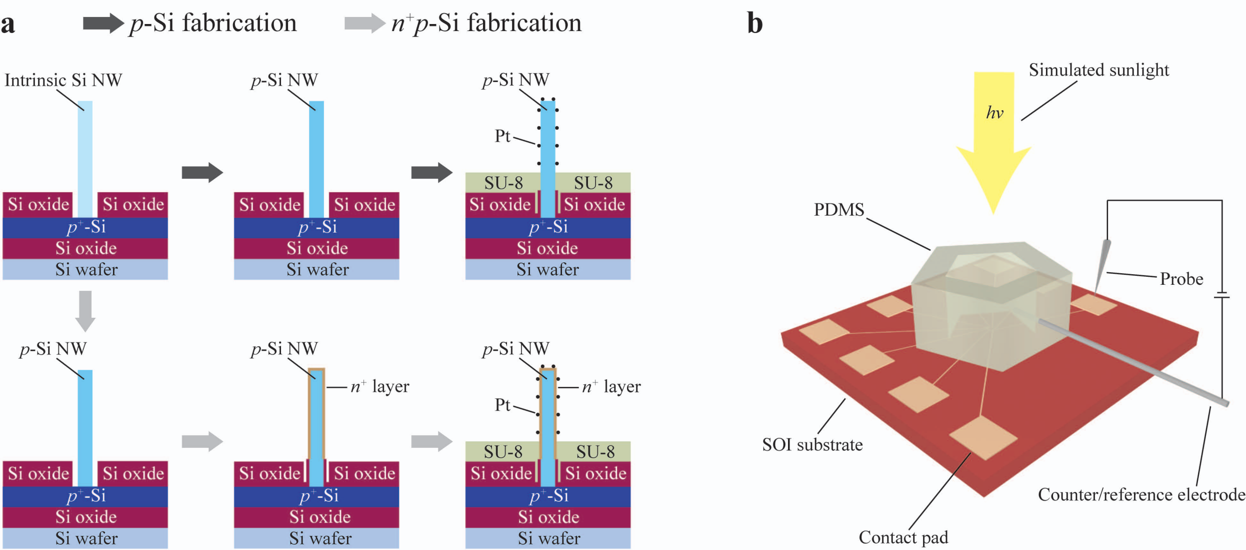
a
p-Si fabrication
n+p-Si fabrication
Intrinsic Si NW
p-Si NW
Pt
SU-8
Si oxide
p+-Si
Si wafer
n+ layer
b
Simulated sunlight
hv
PDMS
Probe
SOI substrate
Contact pad
Counter/reference electrode

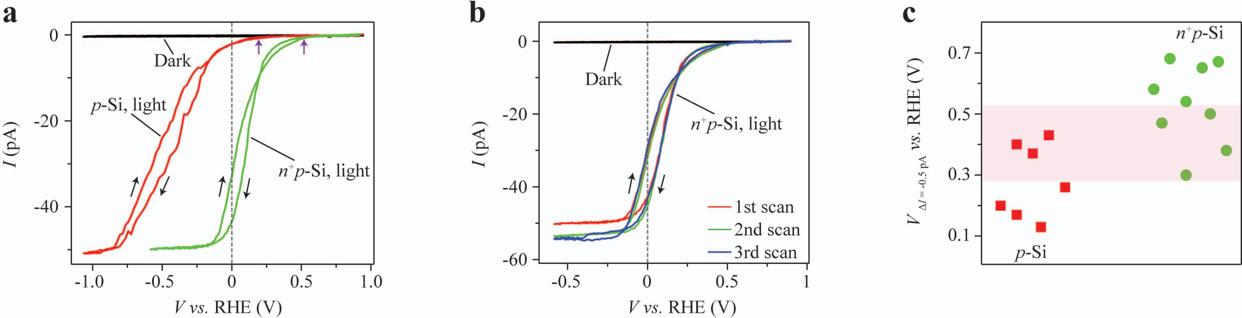

a
0
-20
-40
I (pA)
Dark
p-Si, light
n+p-Si, light
-1.0
-0.5
0
0.5
1.0
V vs. RHE (V)
b
0
-20
-40
-60
I (pA)
Dark
n+p-Si, light
1st scan
2nd scan
3rd scan
-0.5
0
0.5
1
V vs. RHE (V)
c
n+p-Si
p-Si
0.7
0.5
0.3
0.1
V ΔI = -0.5 pA vs. RHE (V)

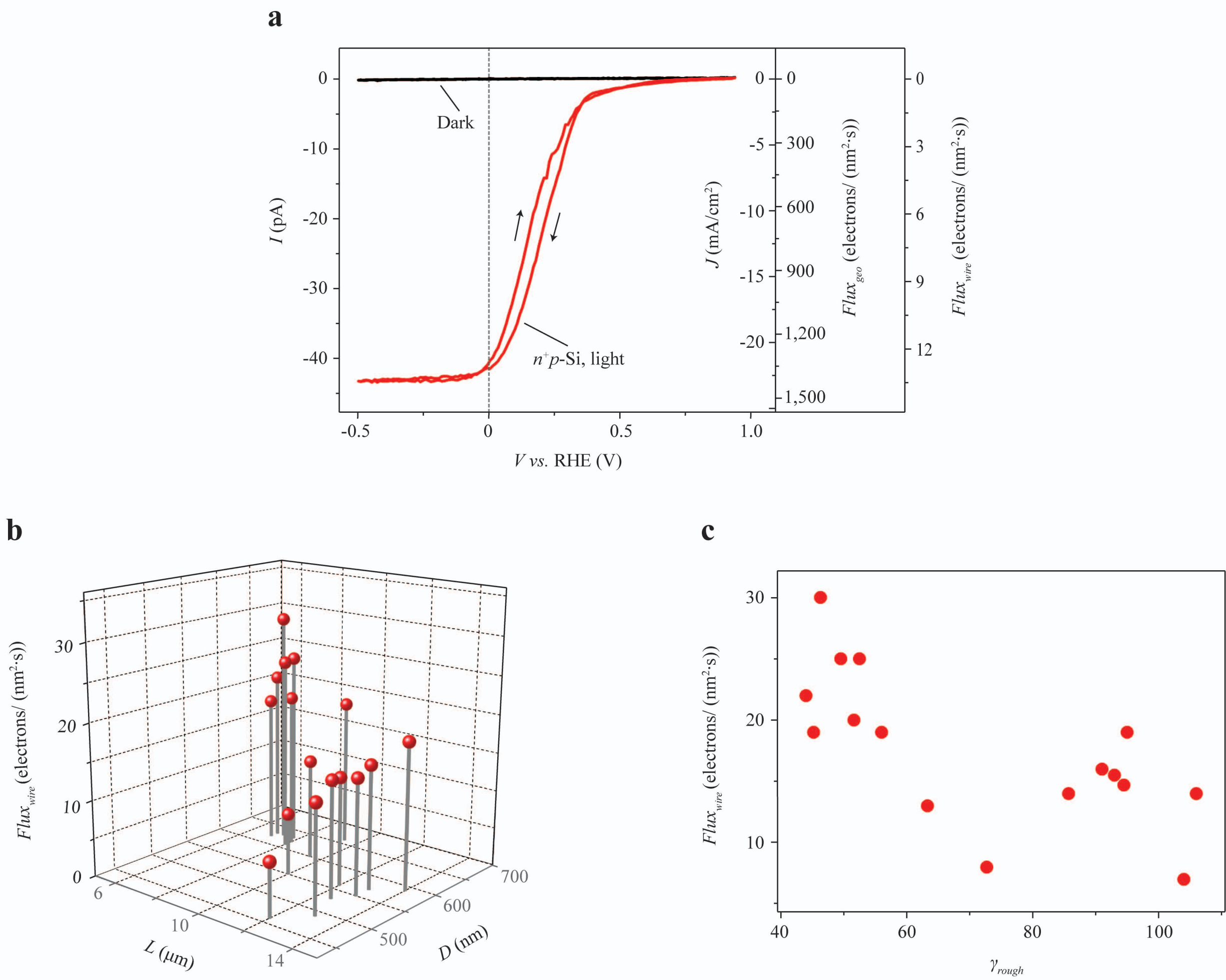
a
0
-10
-20
-30
-40
I (pA)
Dark
n+p-Si, light
-0.5
0
0.5
1.0
V vs. RHE (V)
J (mA/cm2)
-5
-10
-15
-20
300
600
900
1,200
1,500
Flux_geo (electrons/ (nm2·s))
3
6
9
12
Flux_wire (electrons/ (nm2·s))
b
0
10
20
30
Flux_wire (electrons/ (nm2·s))
6
10
14
L (μm)
500
600
700
D (nm)
c
10
20
30
Flux_wire (electrons/ (nm2·s))
40
60
80
100
γ_rough